Pergamon

Available online at www.sciencedirect.com
SCIENCE DIRECT®

Cement and Concrete Research 33 (2003) 899–911

CEMENT AND CONCRETE RESEARCH

Characterisation of crystalline C-S-H phases by X-ray photoelectron spectroscopy

Leon Black[a,*], Krassimir Garbev[a], Peter Stemmermann[a], Keith R. Hallam[b], Geoffrey C. Allen[b]

[a]*Forschungszentrum Karlsruhe GmbH (ITC-WGT), Hermann-von-Helmholtz-Platz 1, Eggenstein-Leopoldshafen 76344, Germany*
[b]*Interface Analysis Centre, University of Bristol, 121 St. Michael's Hill, Bristol, BS2 8BS, England, UK*

Received 18 September 2002; accepted 11 December 2002

Abstract

We have prepared a number of crystalline calcium-silicate-hydrate (C-S-H) phases hydrothermally, with calcium–silicon ratios varying from approximately 0.5 (K-phase) to 2.0 (hillebrandite and α-dicalcium silicate hydrate). The phases were then analysed using X-ray photoelectron spectroscopy (XPS). Increasing calcium–silicon ratios resulted in decreased silicon binding energies. Additionally, changes in the O 1s spectra could be explained in terms of bridging (BO) and nonbridging oxygen (NBO) moieties. Finally, the modified Auger parameter has proved particularly useful in determining the extent of silicate anion polymerisation.

Of note also are the apparently unusual spectra for 11 Å tobermorite. The silicon and oxygen photoelectron spectra indicate a phase with a lower degree of silicate polymerisation than predicted from its composition. The main contributing factor is the intrinsic disorder within the tobermorite structure.

This study has shown how XPS may be used to obtain valuable structural information from C-S-H phases, and our analysis of the crystalline phases is the first step towards the analysis of real C-S-H-based cement systems.

Keywords: Calcium silicate hydrate; Crystal structure; Spectroscopy; XPS

1. Introduction

The phases within the $CaO–SiO_2–H_2O$ system have been extensively studied. Their compositions vary over a large Ca/Si range, and their crystallographic structures range from amorphous to highly crystalline. The former are of immense importance in cement chemistry, where calcium-silicate-hydrate (C-S-H) gels are the principal reaction products and primary binding phases in Portland cement. Such systems contain C-S-H gels with approximate Ca/Si ratios of 1.7, although this ratio fluctuates greatly over the range 0.6 to 2.0 [1]. The precise structures of C-S-H gels have not been fully elucidated, but are related to those of jennite and tobermorite [2,3].

The hydrothermal phases, however, are crystalline, and their structures are well-defined. They may occur, albeit rarely, in nature, or may be formed in autoclaved building materials. As with the amorphous phases, there exists a broad variety of possible structures. The basic building blocks for these minerals are tetrahedral SiO_4^{4-} units, which may link to form one of many structures. There is, of course, a negative charge associated with the silicate structures, which is balanced by the presence of cations, calcium in the case of C-S-H phases.

Thus, with changes in structure and Ca/Si ratio, there are corresponding changes in the bonding states of the elements within the silicate minerals. X-ray photoelectron spectroscopy (XPS) is a technique well suited to examining these changes. When a material is bombarded with X-rays, photoelectrons may be emitted from the topmost surfaces (typically 1–10 nm). The kinetic energies of these photoelectrons may be measured, although convention dictates that kinetic energies are subsequently expressed in terms of binding energy, i.e. the energy required to promote a photoelectron from within an atom to the free state. Each element yields photoelectrons of a specific binding energy, enabling elemental analysis. Additionally, slight changes in the chemical bonding environments result in small shifts in photoelectron energy, thus also enabling chemical information to be obtained. Among the chemical properties which may be

* Corresponding author. Tel.: +49-7247-82-6637.
E-mail address: leon.black@itc-wgt.fzk.de (L. Black).

0008-8846/03/$ – see front matter © 2003 Elsevier Science Ltd. All rights reserved.
doi:10.1016/S0008-8846(02)01089-X

evaluated from the binding energies are oxidation state, electron-spin state, nearest neighbour atoms and type of bonding. More thorough reviews of the technique's capabilities may be found elsewhere [4,5].

Numerous groups have used the surface selectivity of the technique as a means of studying the hydration of calcium silicates [6–10]. To date, however, the full capabilities of this technique, i.e. obtaining bonding information, have not been realised.

Previous studies [6–10] have all used the quantitative capabilities of XPS to study the variation in Ca/Si ratio via changes in the Ca 2p and Si 2p peak intensities. Upon hydration of C_3S [6,10], blast furnace slag [7] and β-C_2S [8], shifts in binding energies were observed, indicating changes in bonding structure. Unfortunately, these results were reported but not commented upon. However, Mollah et al. [11] did relate changes in Si 2p photoelectron spectra to changes in structure. Upon hydration of Portland cement clinker phases, they observed an increase in Si 2p binding energy, tending towards, although not reaching, the binding energy of silica gel. They concluded that these shifts corresponded to an increased polymerisation of the silicate tetrahedra, but not to the extent of forming silica.

Cocke et al. [12] looked at the changes occurring in heavy metal-doped ordinary Portland cement upon leaching. As with Menetrier [9], there was an increase in the O 1s binding energies of approximately 1 eV upon exposure to water. Whereas Menetrier [9] had attributed these changes to the increased presence of –OH, here the increase was attributed to the formation of bridging oxygen (BO) moieties (–Si–O–Si–) as opposed to the more prevalent nonbridging moieties (–Si–O–X–) found in the fresh cement samples. Such observations have also been reported by both Schultz-Münzenberg et al. [13] and Seyama et al. [14]. In both cases, the signals from the bridging and nonbridging moieties were visible as a broadening of the O 1s signal, which could be separated into the two components approximately 2 eV apart. Similarly, Cocke et al. [12] observed a shift of approximately 1.5 eV in the Si 2p peaks upon leaching. This signifies a marked change in structure, corresponding to an increased negative charge upon the silicate structure [15], i.e. loss of charge balancing calcium ions, as was seen in the decrease in intensity of the Ca 2p peak upon leaching.

There have been a few studies examining changes in X-ray photoelectron spectra upon the degradation of various silicate minerals [14–16]. However, an accurate determination of mineral structure is difficult when using X-ray photoelectron peaks alone, due to the small range of chemical shifts and the insulating nature of many silicates. In such instances, a useful means of distinguishing different structures is the concept of the Auger parameter (α), as proposed by Wagner et al. [17,18]. By arranging the Si 2p X-ray photoelectron and Si_{KLL} Auger lines on a two-dimensional plot, better differentiation between compounds may be obtained. The Auger parameter is now more often expressed in its modified form (α') as the sum of the X-ray photoelectron binding energy and the Auger electron kinetic energy, and can be represented on a diagonal grid overlaid on the plot. As the effects of sample charging are equal and opposite for XPS and Auger peaks, α' is independent of charging and can therefore be determined with more accuracy than either line alone. Additionally, α' is a measure of energy changes due to extra-atomic relaxation and is therefore more sensitive to the stoichiometry and strength of bonding to the next nearest neighbours of the emitting atom than XPS binding energy shifts [19]. Such an approach has recently been reported by Okada et al. [20] for a selection of silicate minerals spanning the entire range of silicate polymerisation types, i.e. neso-, iso-, phyllo- and tectosilicates. They observed a clear influence of silicate polymerisation upon both Si 2p binding energy and Si_{KLL} kinetic energy, and related these changes to the effective electrostatic force of Si–O bonds in silicates. Among the minerals investigated by Okada et al. [20] was the calcium silicate wollastonite ($CaSiO_3$). However, despite extensive searches within the literature, we have been unable to find any reference to similar studies of C-S-H.

Despite the efforts of many groups worldwide, there still remains a great deal of work to be done in order to fully understand cement systems. We have attempted to simplify these incredibly complex mixtures by using crystalline C-S-H analogues. In doing so, we are better able to correlate changes in photoelectron spectra with structural changes, and determine how particular factors influence the behaviour of cement systems.

This article presents the first results of an investigation into the suitability of XPS as a means of investigating cement systems. We show that compositional and structural features may be distinguished in the various crystalline phases. This is the first step towards using XPS to study 'real' systems in more detail.

2. Experimental

We prepared numerous crystalline C-S-H phases hydrothermally from stoichiometric mixtures of CaO (freshly prepared from $CaCO_3$ at 1000 °C for 5 h) and SiO_2 (Aerosil). Syntheses were performed under nitrogen atmospheres to avoid carbonation of the C-S-H phases via reactions with atmospheric carbon dioxide. All preparations were two-step processes, beginning with the mechanochemical treatment of the starting materials entailing milling of the oxides together with distilled water (water-to-solid ratio, w/s = 4) in an agate ball mill for 12 h. The mixtures were subsequently treated hydrothermally in Teflon autoclaves. Durations and temperatures of the various hydrothermal treatments are given in Table 1. Finally, all of the samples were allowed to cool to room temperature and dried at 60 °C for 24 h.

Afwillite, α-C_2SH (α-dicalcium silicate hydrate) and C_8S_5 were prepared from β-C_2S which was treated mecha-

Table 1
Hydrothermal handling conditions for the various crystalline phases synthesised for this study

Phase	C/S[a]	Duration	Temperature (°C)
Z-phase	0.5	96 h	170
		plus 16 h	190
Gyrolite	0.66	32 days	220
11 Å Tobermorite	0.83	5 days	170
		plus 5 h	180
Xonotlite	1.00	14 days	220
Foshagite	1.333	16 h	220
Hillebrandite	2.0	7 days	200
Afwillite (plus $Ca(OH)_2$)	2.0[b]	7 days	180
α-C_2SH	2.0[b]	7 days	200
C_8S_5 (plus calcite)	2.0[b]	7 days	220

[a] Indicates the C/S ratio used for synthesis.
[b] Denotes mechanochemically treated β-C_2S.

nochemically in an agate ball mill for 24 h, followed by hydrothermal handling as described above and detailed in Table 1. Formation of pure afwillite was not possible. Rietveld analysis showed the sample consisted of approximately 81% afwillite and 19% portlandite. Similarly, C_8S_5 contained traces of calcite and α-C_2SH traces of kilchoanite and calcite, despite working under an inert atmosphere. Finally, K-phase and truscottite were obtained through thermal treatment of Z-phase and gyrolite, respectively, at 500 °C in air.

The identities and purities of each phase were confirmed both by X-ray diffraction (XRD) and electron microscopy. The phases studied are detailed in Table 2.

Each sample was analysed as received, the powders having been pressed onto adhesive-backed copper tape.

Table 2
Mineral names, formulae and Ca/Si ratios of the C-S-H phases investigated

Phase	Formula	Ca/Si	Reference
Phyllosilicates (sheet silicates comprising $SiO_{2.5}^-$ anionic groups)			
K-phase	$Ca_7(Si_{16}O_{38})(OH)_2$	0.4375	[22]
Z-phase	$Ca_9(Si_8O_{20})_2(OH)_2{\cdot}14H_2O$	0.5625	[21]
Truscottite	$Ca_{14}(Si_8O_{20})(Si_{16}O_{38})(OH)_8{\cdot}2H_2O$	0.5833	[21]
Gyrolite	$Ca_{16}(Si_8O_{20})(Si_8O_{20})_2(OH)_8{\cdot}14H_2O$	0.6666	[21]
Inosilicates (chain silicates comprising SiO_3^{2-} anionic groups)			
11 Å Tobermorite	$Ca_{4.5}(Si_6O_{16})(OH){\cdot}5H_2O$	0.750	[26]
Xonotlite	$Ca_6(Si_6O_{17})(OH)_2$	1.000	[23]
Foshagite	$Ca_4(Si_3O_9)(OH)_2$	1.333	[24]
Hillebrandite	$Ca_2(SiO_3)(OH)_2$	2.000	[25]
Sorosilicates (containing both $Si_3O_{10}^{8-}$ and SiO_4^{4-} anionic groups)			
C_8S_5	$Ca_8(Si_3O_{10})(SiO_4)_2$	1.600	[29]
Nesosilicate (comprising isolated SiO_4^{4-} anionic groups)			
Afwillite ($Ca(OH)_2$ also present)	$Ca_3(SiO_3OH)_2{\cdot}2H_2O$	1.500	[28]
α-C_2SH	$Ca_2(SiO_3OH)(OH)$	2.000	[27]

Table 3
Details of the spectral regions recorded

Region	Start energy (eV)	End energy (eV)
Wide	0	1100
C 1s	275	305
O 1s	520	550
Ca 2p	335	370
Si 2p	90	120
Si 2s	140	163
Si_{KLL} (kinetic energy)	1580	1615

Analysis was performed using a VG Escascope fitted with a MgK_α ($h\nu = 1253.6$ eV) X-ray source operating at 260 W (13 kV, 20 mA). Si_{KLL} Auger lines could be obtained by using the Bremsstrahlung radiation from the Mg source. The intensity of these lines is approximately 20% of that of the Si 2p line [17]. Table 3 gives details of the spectral regions recorded.

Data were extracted from the spectra via peak fitting using XPSPeak software (available by download from: http://www.phy.cuhk.edu.hk/~surface/). A Shirley background was assumed in all cases. An 80:20 Gaussian/Lorentzian peak shape was assumed for photoelectron peaks, while the Auger lines were fitted assuming a 50:50 Gaussian/Lorentzian peak shape. Spectra were corrected for charging effects using the adventitious carbon peak at 284.8 eV.

3. Results and discussion

Typical spectra, together with examples of curve fitting, are shown in Fig. 1, while any trends are discussed below.

3.1. Ca 2p/Si 2p ratio

Very few of the phases could be synthesised in their pure form. Traces of portlandite, ($Ca(OH)_2$) and particularly calcite ($CaCO_3$) were often present, despite our efforts to exclude atmospheric carbon dioxide. Quantification sensitivity factors were obtained empirically, using the peak intensities from xonotlite, which was free of any contamination. Fig. 2 shows a plot of measured Ca/Si ratios versus ideal composition for the phases analysed. The figure shows the calculated Ca/Si ratio both including and excluding the contribution from calcite. For the latter plot, the calcite contributions were calculated using the carbonate peaks within the C 1s spectra and sensitivity factors obtained empirically from a calcite standard.

There is a good linear relationship between ideal and measured composition, as has been observed before for the analysis of C-S-H systems [6–10]. The one obvious outlier is afwillite. However, this phase could not be synthesised in its pure form, and could only be produced intimately mixed with portlandite, hence the higher than expected Ca/Si ratio.

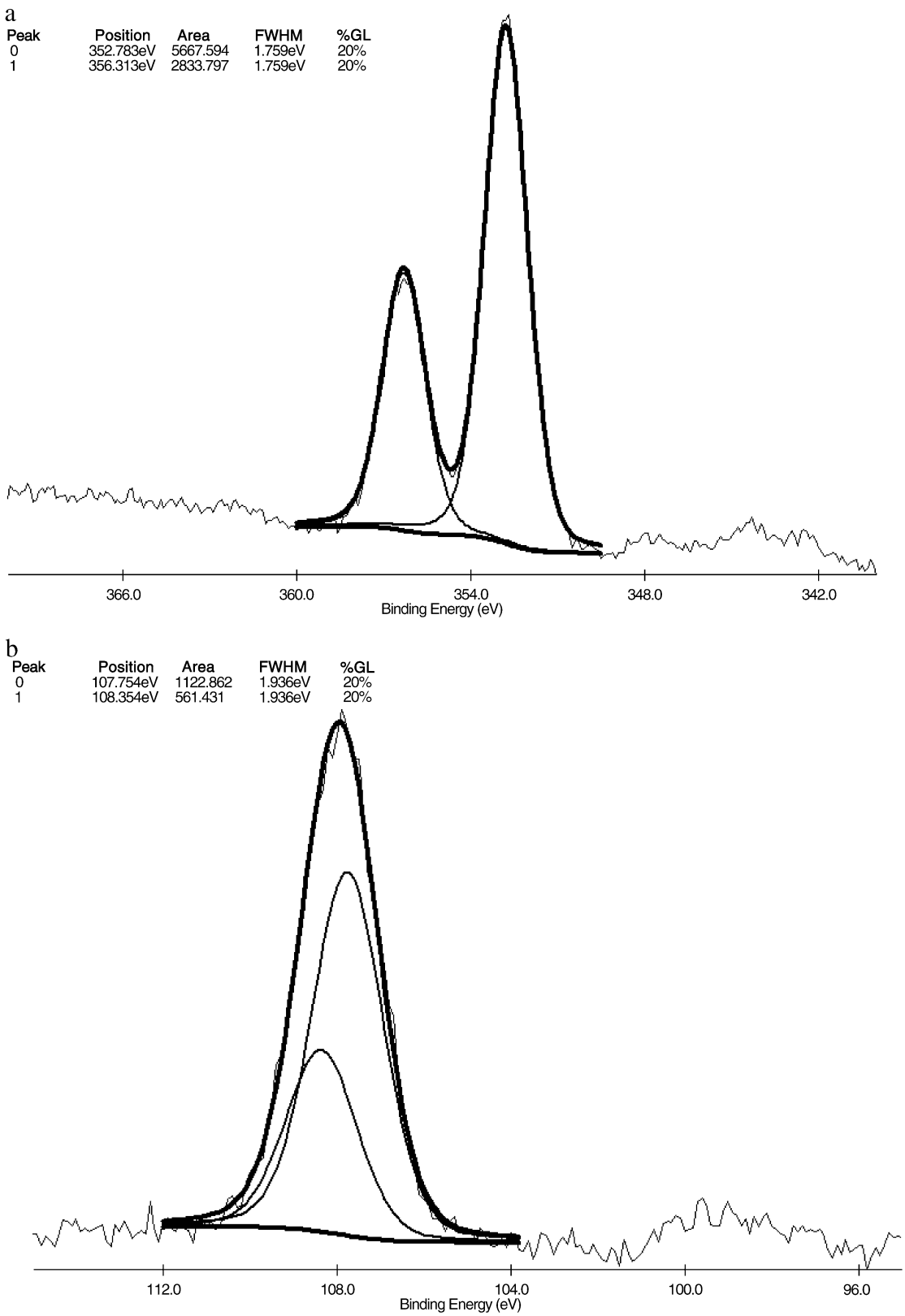

Fig. 1. Examples of typical XPS spectra (xonotlite), including curve fitting results. Note that the data have not been corrected for charging effects. (a) Ca 2p, (b) Si 2p, (c) O 1s, (d) C 1s, (e) Si_{KLL}.

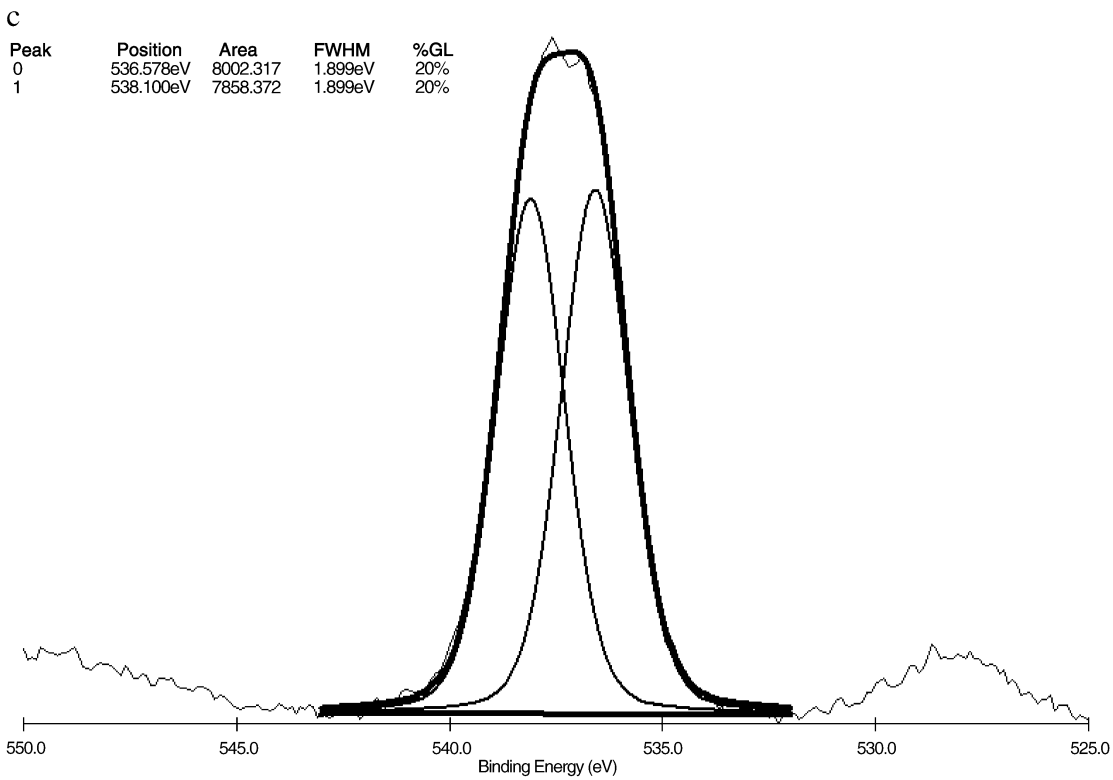

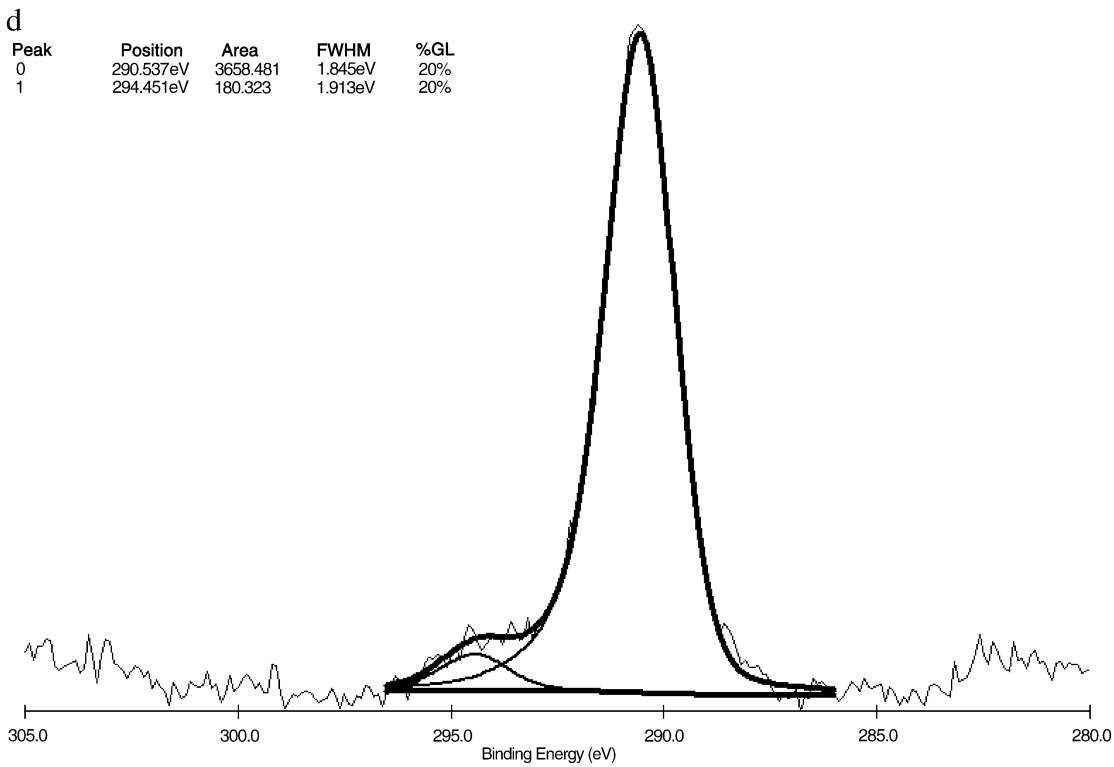

Fig. 1 (*continued*).

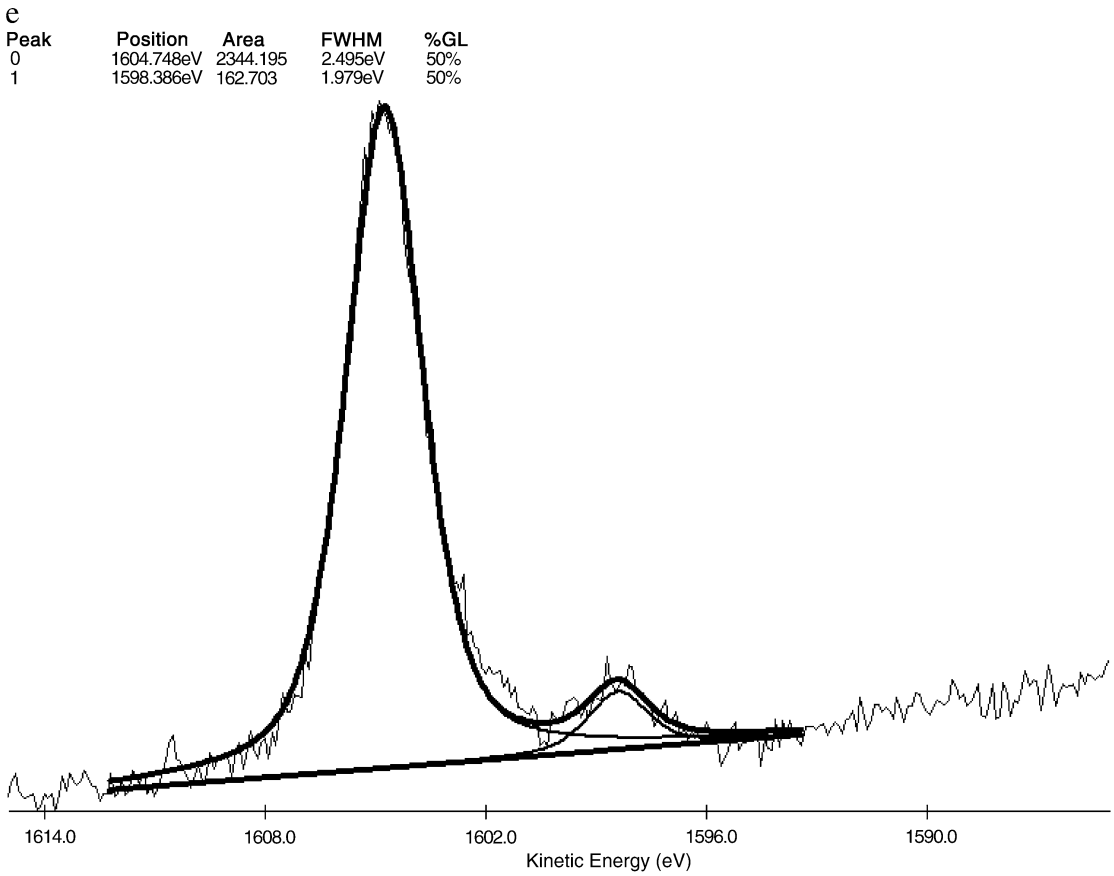

Fig. 1 (*continued*).

3.2. Ca 2p binding energies

Fig. 3 shows a plot of Ca $2p_{3/2}$ binding energies versus Ca/Si ratio. There appears little correlation between the two. These results are in general agreement with Seyama and Soma [15] who found no correlation between binding energy and composition for a number of charge balancing cations within clay systems.

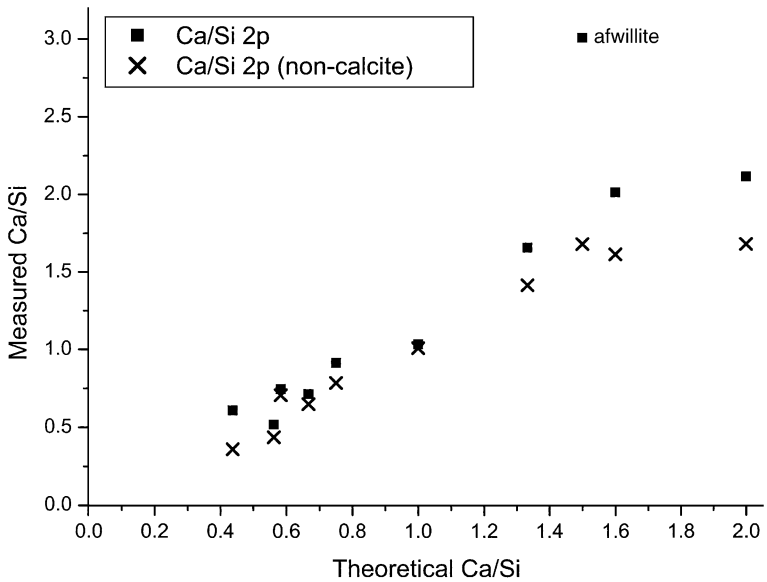

Fig. 2. Plot of measured versus ideal Ca/Si ratio for the phases analysed. Measured Ca/Si ratio indicates that calculated from spectral intensities, while ideal Ca/Si ratio is the theoretical value based upon composition.

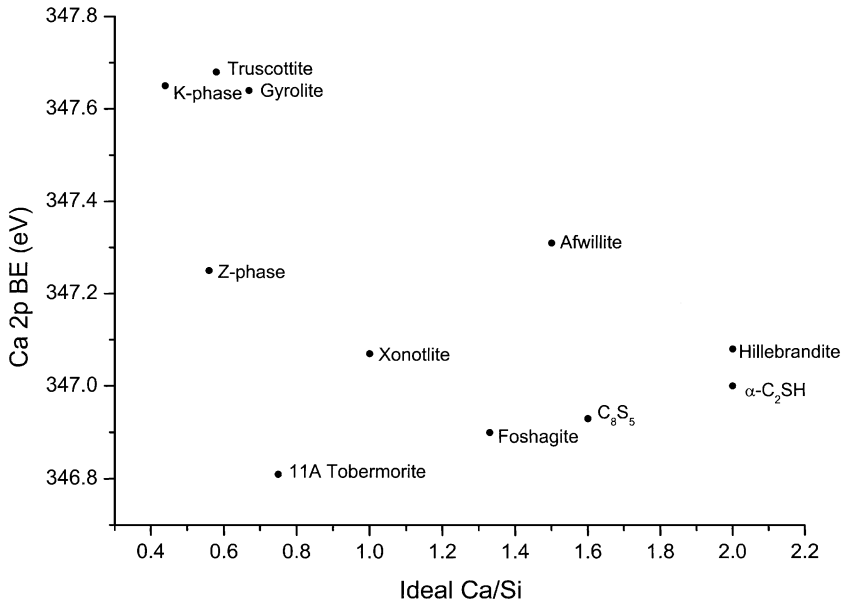

Fig. 3. Plot of Ca $2p_{3/2}$ binding energies versus ideal Ca/Si ratios.

However, the binding energies of calcium depleted phases (the phyllosilicates) were generally higher than the others, which made us examine the results more closely and led us to believe that calcium coordination number rather than simply Ca/Si ratio was an important factor. Calcium is always sixfold coordinated in the phyllosilicates, [21,22]. It may be six or sevenfold coordinated in many of the inosilicates (xonotlite [23], foshagite [24] and hillebrandite [25]), with the exception of 11 Å tobermorite [26], which contains only sevenfold coordinated calcium atoms. Meanwhile, crystalline nesosilicate C-S-H phases may consist either of six- and sevenfold coordinated calcium as in α-dicalcium silicate hydrate [27] or only sevenfold coordinated calcium as in afwillite [28]. Finally, the sorosilicate C_8S_5 (structurally related to kilchoanite) contains both sixfold and eightfold coordinated calcium [29]. Thus, Fig. 4 shows a plot of Ca $2p_{3/2}$ binding energy versus the average calcium coordination number for each of the phases analysed. This plot shows how the calcium coordination number has a slight influence upon binding energy. A lower coordination number leads to

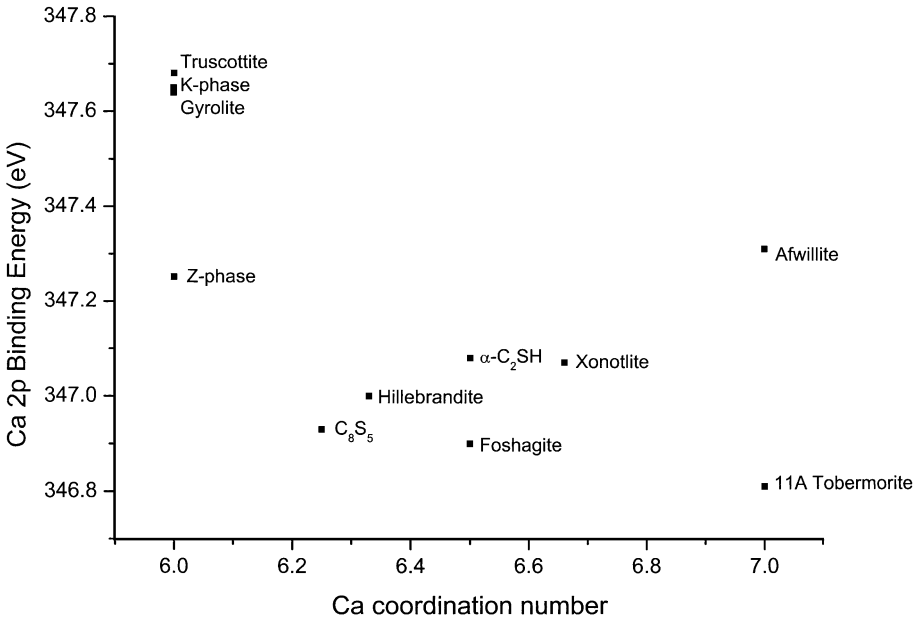

Fig. 4. Plot of Ca $2p_{3/2}$ binding energy versus the average calcium coordination number as obtained from structural determinations.

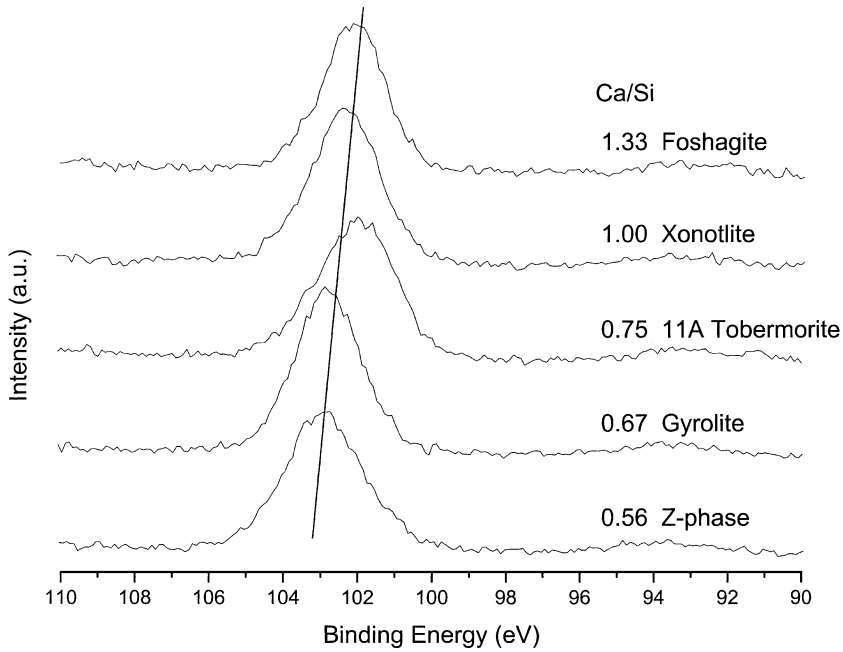

Fig. 5. A selection of Si 2p photoelectron spectra recorded from various crystalline C-S-H phases used in this study. Note that the abscissa runs in the negative direction according to convention.

a shorter, stronger Ca–O bond and thus a higher binding energy.

3.3. Silicon binding energies

Both the Si 2p and Si 2s lines were measured for each sample. The Si 2p lines are commonly measured, these being sharper and more intense than the Si 2s lines. However, other authors report problems measuring the former when using an aluminium Kα X-ray source [14,15,30]. Therefore, to enable ready comparisons between our results and others, we measured both sets of lines. Trends were equally evident in both sets of lines.

Fig. 5 shows a selection of Si 2p XPS spectra obtained in this study, while Fig. 6 shows a plot of both Si $2p_{3/2}$ and Si 2s binding energies versus Ca/Si ratio. There is a clear decrease in binding energy with increasing calcium content. This may be understood by remembering that calcium acts as a charge-balancing cation within the C-S-H structure. Higher Ca/Si ratios imply higher residual negative charges

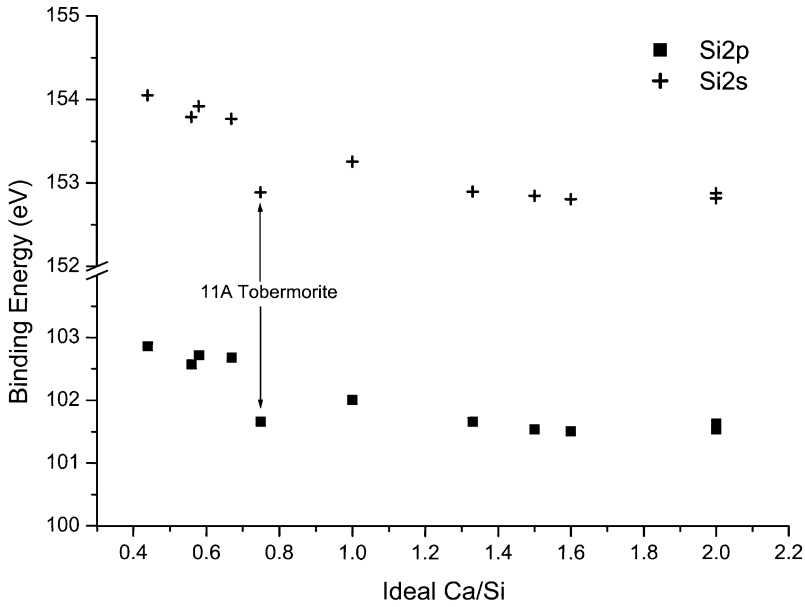

Fig. 6. Plot of both Si $2p_{3/2}$ and Si 2s binding energies versus ideal Ca/Si ratios.

on the silicate tetrahedra, thus the silicon atoms are subjected to increased screening and relaxation, in turn leading to a lower binding energy. A similar relationship was reported by Seyama and Soma [15] and Carriere and Deville [31], who both showed a relationship between the anionic O/Si ratio and silicon binding energies (Si 2s and Si 2p for Seyama and Soma [15] and Carriere and Deville [31], respectively). As the anionic O/Si ratio decreased from 4 (for nesosilicates), via 3 (inosilicates) to 2.5 (phyllosilicates) and eventually 2 (silica), the silicon binding energies increased.

11 Å Tobermorite has a binding energy much lower than that predicted from its Ca/Si ratio, as seen in Figs. 5 and 6, the cause of which is worthy of some explanation. The main contributing factor is the intrinsic disorder within the tobermorite structure caused by the variation in the calcium content of the so-called zeolitic position (Ca_2 using the notation of Merlino et al. [26]). It is widely accepted that the variation in the calcium content (C/S = 4/6–5/6) (by one atom per unit formula) has a great effect on the coordination of Si_2. With low calcium contents (C/S = 4/6), the nonbridging oxygen atoms (NBOs) of the bridging Si-tetrahedra (O_6) are hydroxylated. With increasing C/S ratios, the "zeolitic" position is progressively occupied, creating an excess of positive charge, which is compensated for by a loss of protons, until at full calcium occupation there is full occupation of position O_6 by oxygen. In the structure determination of 11 Å tobermorite from the Urals (C/S ratio = 4.5/6), the bond length Si–O_6 is fairly long (ca. 1.68 Å) [26].

Molecular dynamics simulations by Faucon et al. [32] have shown that with increasing C/S ratio rupture of the tetrahedral chains can occur between bridging and nonbridging silicon atoms, thus forming isolated pyrogroups $[Si_2O_7]^{6-}$. This model is validated through ^{29}Si NMR results which show between 10% and 20% Q^1 in the spectra [33]. In this sense, 11 Å tobermorite should not be classified as a strictly chain silicate, and may be regarded as less polymerised than xonotlite in terms of condensation of Si-tetrahedra.

Another indication of decreased polymerisation in 11 Å tobermorite is the occurrence of polytypes with single chains of wollastonite type (so-called dreiereinfachketten) [34]. The presence of such chains indicates that the double chains within tobermorite are not as stable as the double chains in xonotlite. Additionally, the possibility of exchanging aluminium for silicon in tobermorite (up to 1/6 of all silicon atoms), but not in xonotlite, resulting in increased stability of the former with respect to xonotlite [35], again is indicative of tobermorite's instability.

The unusually low binding energy of 11 Å tobermorite is also reflected in its thermodynamic instability. Over the temperature range 170–200 °C, it is metastable with respect to both gyrolite (lower C/S ratio) and xonotlite (higher C/S ratio), both of which have more highly polymerised Si-tetrahedra.

3.4. Si_{KLL} Auger peaks

The principal reason for recording the Si_{KLL} Auger line was to determine the modified Auger parameter (vide infra). However, the results are interesting in their own right. An advantage of using this line over the photoelectron lines is that the shift is much greater, more than compensating for the slightly broader peaks.

Fig. 7 shows the variation in kinetic energy with Ca/Si ratio. There is a gradual increase in kinetic energy with

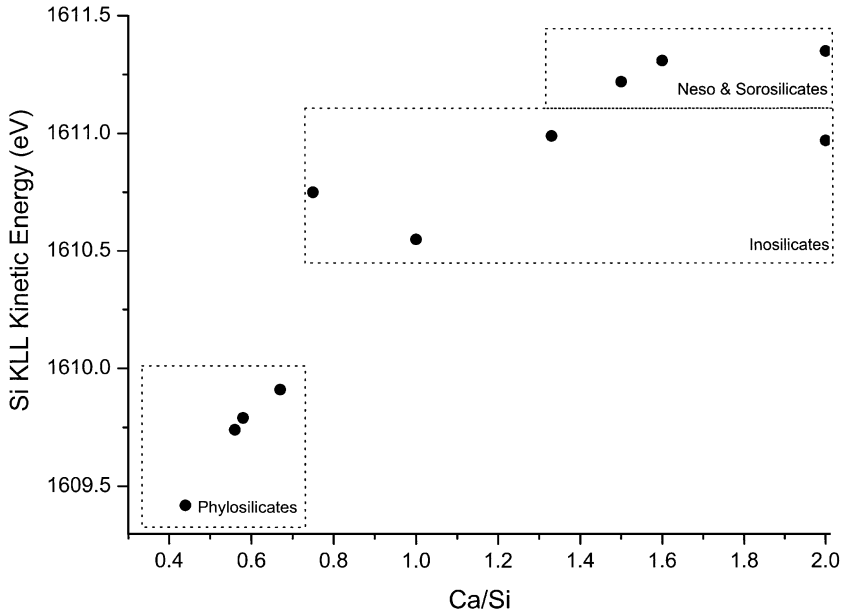

Fig. 7. Plot of Si_{KLL} kinetic energy versus ideal Ca/Si ratios.

increasing Ca/Si ratios. However, this simplified interpretation shows a number of outliers. It is better to consider the results in three groups, separated according to silicate structure. The phyllosilicates may be represented as $SiO_{2.5}^{1-}$, thus there is only a small charge on each silicon tetrahedron and minimal relaxation, hence the low kinetic

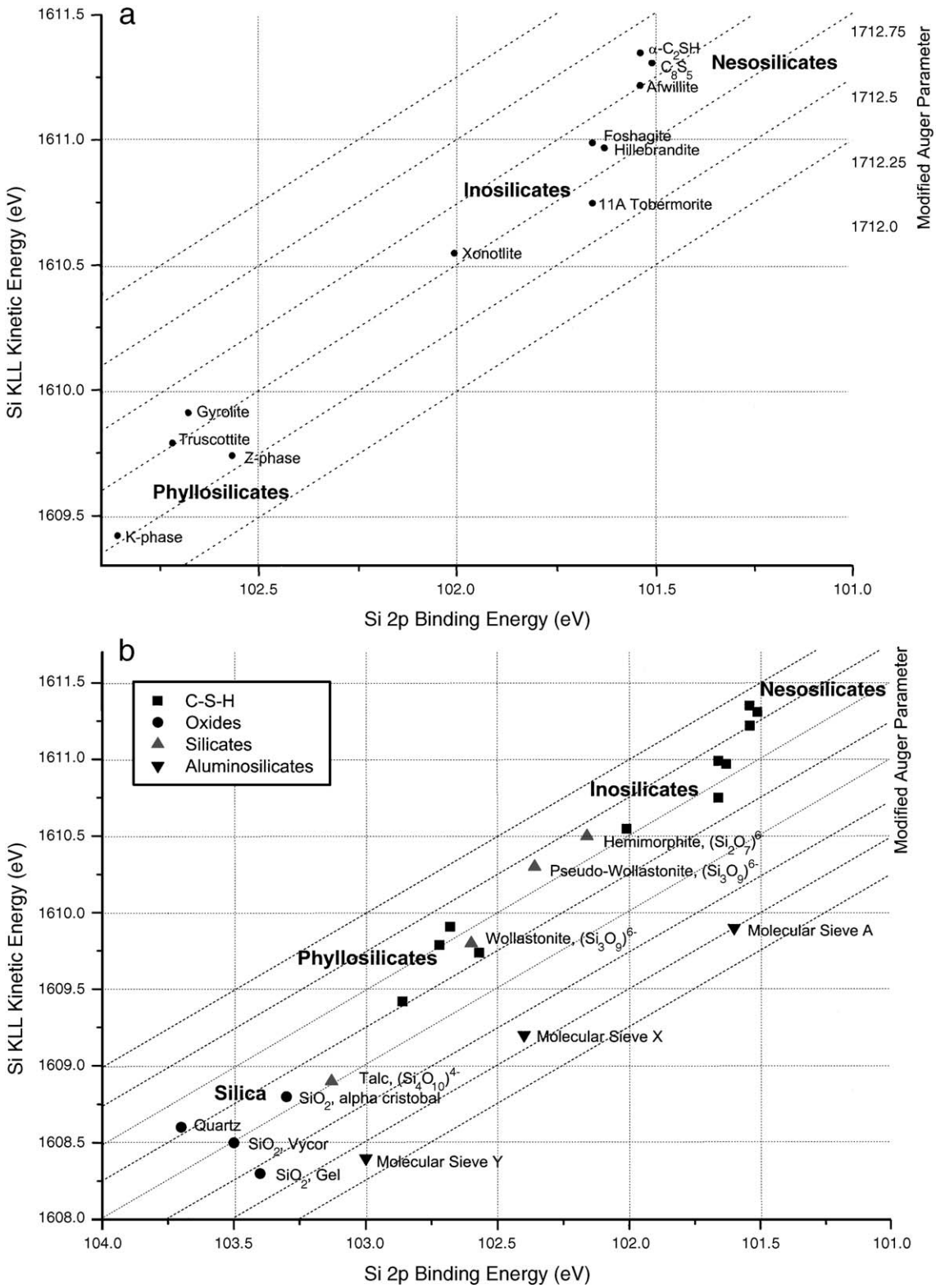

Fig. 8. 2-D chemical state plot of Si 2p binding energy versus Si_{KLL} kinetic energy. Equivalent modified Auger parameter values (α') lie along the diagonals. (a) The data for the phases studied; (b) a number of other silicate phases for comparison.

energy. The inosilicates posses a structure which may nominally be written thus: SiO_3^{2-}. There is a higher residual charge on each silicate tetrahedron than for the phyllosilicates, hence greater relaxation around the silicon atoms resulting in higher kinetic energies. Finally, the nesosilicates comprised of isolated tetrahedra may be represented, thus: SiO_4^{4-}. They exhibit the greatest degree of relaxation, thus the highest Si_{KLL} kinetic energies.

3.5. Modified Auger parameter

The measurement of the modified Auger parameter (α') has two advantages with regards to our work. Firstly, α' is a measure of energy changes due to extra-atomic relaxation and is therefore more sensitive to the stoichiometry and bonding state than XPS binding energy shifts alone [19]. Secondly, errors due to surface charging are removed by the equal and opposite shifts in each of the two contributing energies.

Fig. 8a shows the 2-D chemical state plot for the phases studied. The plot is of Si $2p_{3/2}$ binding energy versus Si_{KLL} kinetic energy, with equivalent α' values lying along the diagonals. Unfortunately, the literature regarding the determination of α' for mineral phases is very sparse. Hence, comparisons with the results of others are difficult. However, the above plot is repeated in Fig. 8b, with the addition of a number of other silicate phases for comparison (data adapted from Refs. [17,19,20,36]). These plots allow more ready differentiation between the different phases than plots of either photoelectron binding energy or Auger electron kinetic energy alone. Additionally, grouping of phases with similar structures can be seen. The phyllosilicates may be easily differentiated from the other phases by photoelectron binding energies alone, but the 2-D plots shown in Fig. 8a and b also allow ready differentiation between the inosilicates and nesosilicates. The latter group of compounds possesses α' values higher than the former (and the phyllosilicates), a reflection of the greatly different silicon bonding arrangement. The value for C_8S_5 meanwhile lies between those of the neso- and inosilicates, a result of its structure, being a sorosilicate containing both Si_3O_{10} and SiO_4 silicate anions. The α' values for the various inosilicates and phyllosilicates are similar, indicative perhaps of their similar polymeric structures. The nesosilicates meanwhile are well separated from the rest, a result of their isolated silicate tetrahedra. This may perhaps be more clearly seen in Fig. 9, where α' values are plotted against Ca/Si ratio.

3.6. O 1s binding energies

Putnis [37] states that the Si–O bond lengths of BOs are about 0.025 Å longer than of nonbridging atoms. This increased bond length is reflected in an increased photoelectron binding energy, as shielding of the silicon atoms decreases, as has been seen by both Seyama et al. [14] and Schultz-Münzenberg et al. [13]. The presence of water of crystallisation and hydroxide groups, together with both BO and NBO groups, makes quantitative analysis difficult. However, trends are still evident as may be clearly seen in Fig. 10. This plot shows a selection of O 1s spectra from the crystalline phases used in this study. With increasing Ca/Si ratio, there is an increased contribution from the NBOs, seen as a change in the symmetry of the spectra. Attempts at quantification, however, were not successful, and more

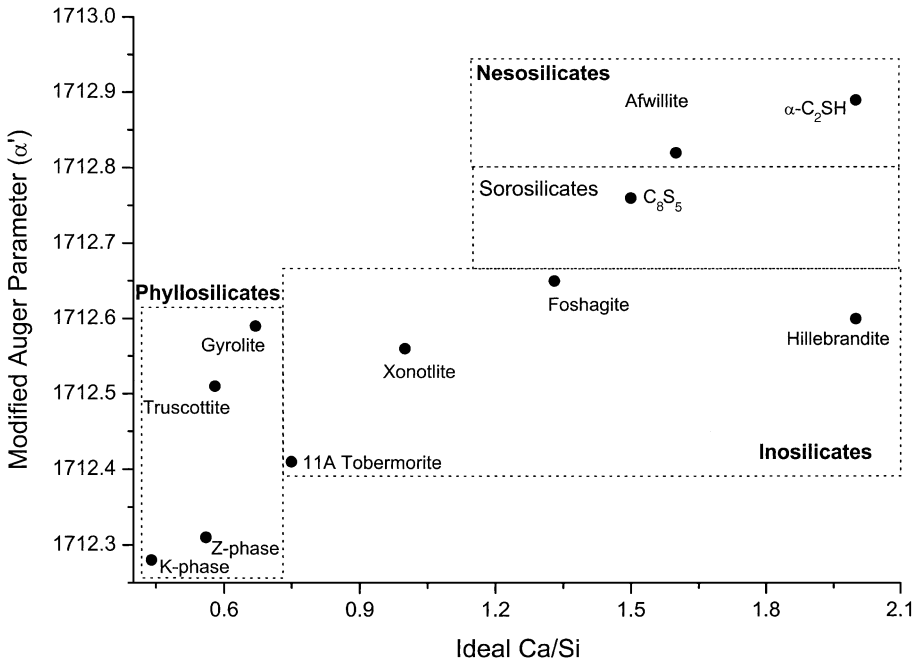

Fig. 9. Plot of modified Auger parameter (α') versus ideal Ca/Si ratios.

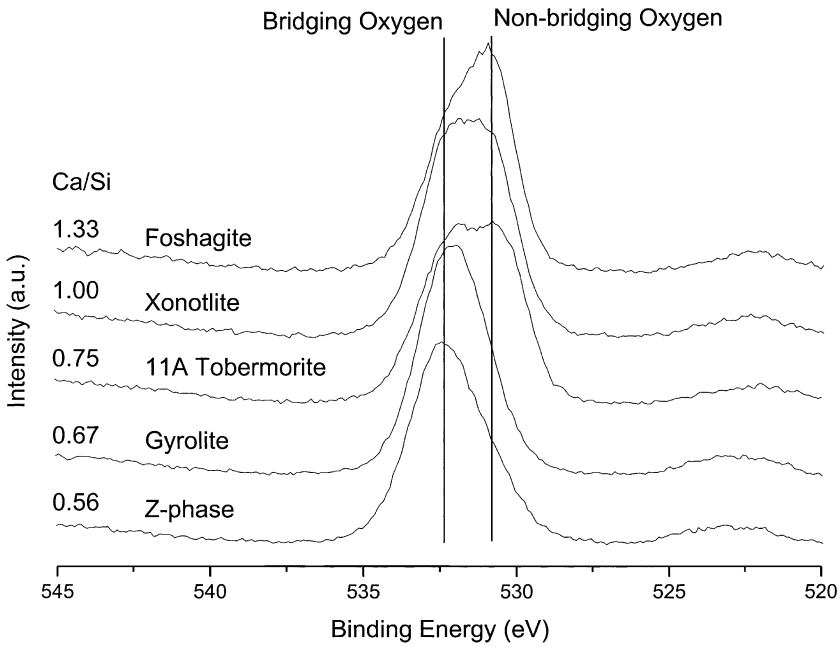

Fig. 10. A selection of O 1s photoelectron spectra recorded from various crystalline C-S-H phases used in this study. The tendency towards the increased prevalence of NBOs with increasing Ca/Si ratio is clear.

work is required in this area to distinguish the contributions from BOs, NBOs, hydroxide anions and water of crystallisation.

Again, differences between the spectra are the result of changes in C-S-H structure. Thus, XPS may be used to characterise crystalline C-S-H phases. Higher Ca/Si ratios lead to an increased preponderance of NBOs, which themselves bond to the charge balancing calcium ions thus, Ca–O–Si.

4. Conclusions

X-ray photoelectron spectroscopy has been shown to be a useful tool for characterising various crystalline calcium silicate hydrate phases. Via a combination of different spectral parameters, we have been able to identify differences in silicate structure for different phases. Structural changes are revealed via changes in the photoelectron spectra in a number of ways, as summarised below:

- XPS is quantitative. Therefore, changes in Ca/Si ratios are reflected in the ratios of their photoelectron peak intensities.
- Calcium binding energies are relatively independent of C-S-H composition or structure. However, at low Ca/Si ratios, the binding energies are slightly higher, as a result of both the slightly shorter Ca–O bonds between the silicate anions and the calcium ions and the decreased calcium coordination in these compounds.
- Both Si 2p and Si 2s binding energies showed a dependence upon composition. Higher Ca/Si ratios imply a higher residual negative charge upon the silicate tetrahedra. This results in increased screening and relaxation of silicon atoms, leading to lower binding energies.
- The trends in silicon photoelectron binding energies may also be understood in terms of the O/Si ratio of the silicate anions. As the O/Si ratio decreases, the silicon binding energy increases. This may be explained as above.
- The Si_{KLL} kinetic energies increased with increasing Ca/Si ratio. A plot of kinetic energy versus Ca/Si ratio reveals three regions, according to silicate structure, i.e. phyllosilicate, inosilicate and nesosilicate.
- The different phases could be distinguished best of all via the modified Auger parameter (α'). This is ideally displayed using a 2-D chemical state plot of Si_{KLL} kinetic energies versus Si 2p binding energies. Equivalent values of α' lie along the same diagonal.
  The greatly different structure of the nesosilicates was reflected in higher values of α'. The phyllosilicates and inosilicates were better distinguished via the 2-D plots.
- BOs and NBOs may be distinguished via their O 1s binding energies. The presence of water of crystallisation, hydroxyl groups and adsorbed water made quantitative analysis impossible, and curve fitting allows only semi-quantitative analysis of the ratio of NBO to BO atoms in various phases. Increased Ca/Si ratios lead to an increased NBO/BO ratio. Problems are encountered due to the presence of hydroxide groups and water of crystallisation.
- The binding energies for tobermorite deviate from their expected values. These may be explained by considering the intrinsic disorder within the tobermorite structure and the presence of isolated pyrogroups $[Si_2O_7]^{6-}$ as a result of rupture of silicate chains.

To date, we have investigated crystalline C-S-H phases as crystalline analogues of the very important amorphous C-S-H phases found in cement systems. We have shown how XPS may be used to distinguish the various phases, and how the spectra may be influenced by the silicate structure. It is therefore hoped that XPS may now be applied to 'real' cement systems, furthering the understanding of the composition, structure and stability of such systems.

Acknowledgements

We acknowledge the support of the European Community Access to Research Infrastructure action of the Improving Human Potential Programme, contract HPRI-CT-1999-00008 awarded to Prof. B.J. Wood (EU Geochemical Facility, University of Bristol).

References

[1] X. Zhang, W. Chang, T. Zhang, C.K. Ong, Nanostructure of calcium silicate hydrate gels in cement paste, J. Am. Ceram. Soc. 83 (10) (2000) 2600–2604.
[2] H.F.W. Taylor, Cement Chemistry, Academic Press, London, 1990.
[3] R.J. Kirkpatrick, J.L. Yarger, P.F. McMillan, P. Yu, X. Cong, Raman spectroscopy of C-S-H, tobermorite and jennite, Adv. Cem. Based Mater. 5 (1997) 93–99.
[4] D. Briggs, M.P. Seah, Practical Surface Analysis, 2nd ed., Auger and X-ray Photoelectron Spectroscopy, vol. 1, Wiley, Chichester, UK, 1994.
[5] M.F. Hochella Jr., Auger electron and X-ray photoelectron spectroscopies, in: F.C. Hawthorne (Ed.), Reviews in Mineralogy, Spectroscopic Methods in Mineralogy and Geology, vol. 18, Mineralogical Society of America, Washington, DC, 1988, pp. 573–637.
[6] M. Regourd, J.H. Thomassin, P. Baillif, J.C. Touray, Study of the early hydration of Ca_3SiO_5 by X-ray photoelectron spectrometry, Cem. Concr. Res. 10 (1980) 223–230.
[7] M. Regourd, J.H. Thomassin, P. Baillif, J.C. Touray, Blast furnace slag hydration, surface analysis, Cem. Concr. Res. 13 (1983) 549–556.
[8] J.H. Thomassin, M. Regourd, P. Baillif, J.C. Touray, Étude de l'hydratation initiale du silicate bicalcique β par spectrométrie de photoélectrons, C. R. Acad. Sci. Paris 290 (Jan. 1980) 1–3.
[9] D. Menetrier, I. Jawed, T.S. Sun, J. Skalny, ESCA and SEM studies on early C_3S hydration, Cem. Concr. Res. 9 (1979) 473–482.
[10] S. Long, C. Liu, Y. Wu, ESCA Study on the early C_3S hydration in NaOH solution and pure water, Cem. Concr. Res. 28 (2) (1998) 245–249.
[11] M.Y.A. Mollah, T.R. Hess, Y.-N. Tsai, D.L. Cocke, An FTIR and XPS investigations of the effects of carbonation on the solidification/stabilization of cement based systems—Portland type V with zinc, Cem. Concr. Res. 23 (1993) 773–784.
[12] D.L. Cocke, M.Y.A. Mollah, J.R. Parga, T.R. Hess, J.D. Ortago, An XPS and SEM/EDS characterization of leaching effects on lead- and zinc-doped Portland cement, J. Hazard. Mater. 30 (1992) 83–95.
[13] C. Schultz-Münzenberg, W. Meisel, P. Gütlich, Changes of lead silicate glasses induced by leaching, J. Non-Cryst. Solids 238 (1998) 83–90.
[14] H. Seyama, M. Soma, A. Tanaka, Surface characterization of acid-leached olivines by X-ray photoelectron spectroscopy, Chem. Geol. 129 (1996) 209–216.
[15] H. Seyama, M. Soma, Bonding-state characterization of the constituent elements of silicate minerals by X-ray photoelectron spectroscopy, J. Chem. Soc., Faraday Trans. 81 (1985) 485–495.
[16] K.V. Ragnasdottir, C.M. Graham, G.C. Allen, Surface chemistry of reacted heulandite determined by SIMS and XPS, Chem. Geol. 131 (1996) 167–181.
[17] C.D. Wagner, D.E. Passoja, H.F. Hillery, T.G. Kinsky, H.A. Six, W.T. Jansen, J.A. Taylor, Auger and photoelectron line energy relationships in aluminium–oxygen and silicon–oxygen compounds, J. Vac. Sci. Technol. 21 (4) (1982) 933–944.
[18] C.D. Wagner, A. Joshi, The Auger parameter, its utility and advantages: a review, J. Electron Spectrosc. Relat. Phenom. 47 (1988) 283–313.
[19] M. Steveson, P.S. Arora, R.St.C. Smart, XPS studies of low-temperature plasma-produced graded oxide–silicate–silica layers on titanium, Surf. Interface Anal. 26 (1998) 1027–1034.
[20] K. Okada, Y. Kameshima, A. Yasumori, Chemical shifts of silicon X-ray photoelectron spectra by polymerization structures of silicates, J. Am. Ceram. Soc. 81 (7) (1998) 1970–1972.
[21] S. Merlino, Gyrolite: its crystal structure and crystal chemistry, Mineral. Mag. 52 (1988) 377–387.
[22] J.A. Gard, K. Luke, H.F.W. Taylor, The crystal structure of K-phase $Ca_7Si_{16}O_{40}H_2$, Kristallografiya 26 (1981) 1218–1223.
[23] Y. Kudoh, Y. Takeuchi, Polytypism of xonotlite: 1. Structures of an A-1 polytype, Mineral. J. (Japan) 9 (1979) 349–373.
[24] J.A. Gard, H.F.W. Taylor, The crystal structure of foshagite, Acta Crystallogr. 13 (1960) 785–793.
[25] Y. Dai, J.E. Post, Crystal structure of hillebrandite: a natural analogue of calcium silicate hydrate CSH phases in Portland cement, Am. Mineral. 80 (1995) 841–844.
[26] S. Merlino, E. Bonacorssi, T. Armbruster, Tobermorites: their real structure and order–disorder (OD) character, Am. Mineral. 84 (1999) 1613–1621.
[27] R.E. Marsh, A revised structure for α-dicalcium silicate hydrate, Acta Crystallogr. C 50 (1994) 996–997.
[28] K.M.A. Malik, J.W. Jefferey, A re-investigation of the structure of afwillite, Acta Crystallogr. 32 (1976) 475–480.
[29] H.F.W. Taylor, The crystal structure of kilchoanite $Ca_6(SiO_4)(Si_3O_{10})$ with some comments on related phases, Mineral. Mag. 38 (1971) 26–31.
[30] T.A. Clarke, E.N. Rizkalla, X-ray photoelectron spectroscopy of some silicates, Chem. Phys. Lett. 37 (3) (1976) 523–526.
[31] B. Carriere, J.P. Deville, X-ray photoelectron study of some silicon–oxygen compounds, J. Electron Spectrosc. Relat. Phenom. 10 (1977) 85–91.
[32] P. Faucon, J.M. Delaye, J. Virlet, J.F. Jacquinot, F. Adenot, Study of the structural properties of the C-S-H(I) by molecular dynamics simulation, Cem. Concr. Res. 27 (10) (1997) 1581–1590.
[33] Y. Okada, H. Ishida, T. Mitsuda, ^{29}Si NMR spectroscopy of silicate anions in hydrothermally formed C-S-H, J. Am. Ceram. Soc. 77 (1994) 765–768.
[34] S.A. Hamid, The crystal structure of the 11 Å natural tobermorite $Ca_{2.25}[Si_3O_{7.5}(OH)_{1.5}]\cdot 2H_2O$, Z. Kristallogr. 154 (1981) 189–198.
[35] S. Shaw, S.M. Clark, C.M.B. Henderson, Hydrothermal formation of the calcium silicate hydrates tobermorite ($Ca_5Si_6O_{16}(OH)_2.4H_2O$) and xonotlite ($Ca_6Si_6O_{17}(OH)_2$): an in-situ synchrotron study, Chem. Geol. 167 (2000) 129–140.
[36] J.F. Moulder, W.F. Stickle, P.E. Sobol, K.D. Bomben, in: J. Chastain (Ed.), Handbook of X-ray Photoelectron Spectra—A Reference Book of Standard Spectra for Identification and Interpretation of XPS Data, Perkin-Elmer, Eden Prairie, MN, 1992.
[37] A. Putnis, Introduction to Mineral Sciences, 4th ed., Cambridge Univ. Press, Cambridge, 1992.